INERTIA-DEPENDENT SCALING OF PARTICLE CLUSTERING AND SPREADING IN AXISYMMETRIC REATTACHMENT FLOWS

Giuseppe A. Rosi
giuseppe-antonio.rosi@tu-bs.de
Institute of Fluid Mechanics
TU Braunschweig
Hermann-Blenk-Straße 37
38108 Braunschweig, DE

İlber D. U. Ceylan
Institute of Fluid Mechanics
TU Braunschweig
Hermann-Blenk-Straße 37
38108 Braunschweig, DE

Filippo G. Colombo
Institute of Fluid Mechanics
TU Braunschweig
Hermann-Blenk-Straße 37
38108 Braunschweig, DE

David E. Rival
Institute of Fluid Mechanics
TU Braunschweig
Hermann-Blenk-Straße 37
38108 Braunschweig, DE

Georg Garnweitner
Institute of Particle Technology
TU Braunschweig
Volkmaroder Straße 5
38104 Braunschweig, DE

BACKGROUND

In suspension flows, interactions between suspended particles and the carrier phase promote both dissipation (energy extraction) and diffusion (scale broadening) of coherent flow structures. Dissipation—the attenuation of kinetic disturbances by the suspended phase—is a laminar-like behavior that stabilizes the flow and has motivated effective-viscosity frameworks that increase energy decay (Stickel & Powell, 2005; Guazzelli & Pouliquen, 2018). Dissipation through particle loading has been observed through suppression of turbulent spots during transition (Hogendoorn & Poelma, 2018), and attenuation of hairpin vortices in wall-bounded turbulence (Kiger & Pan, 2002; Richter & Sullivan, 2014). Concurrently, particle loading enhances diffusion—improved mixing and momentum transfer—a turbulent-like response (Druzhinin, 1994; Shuai & Kasbaoui, 2022). This behavior is observed in confined vortex rings of dense suspensions, where the vortex core and associated fluctuations diffuse rapidly, producing a broader, more stable structure despite classical predictions of greater instability (Zhang & Rival, 2020; Barnes *et al.*, 2024). Both tendencies—dissipation and diffusion—have been documented in sudden-expansion flows: shear-layer dissipation reduces freestream entrainment (Jeronimo & Rival, 2021), yet shorter reattachment lengths comparable to turbulent flows would suggest increased wall-normal momentum transfer (Rosi *et al.*, 2025). These observations point to a dual role of suspended particles: attenuating coherent structures while simultaneously enhancing momentum transfer.

Missing from this dual description is how particle characteristics—particularly inertia—govern the balance between these competing effects. Even for very small particles, the resulting dynamics remain complex and unclear. In the point-particle regime, low-inertia particles closely follow coherent flow structures, modulating them in a largely isotropic, monotonic manner while preserving the single-phase energy cascade. In contrast, high-inertia particles decouple from flow structures, enhancing energy transfer from large to small scales in an anisotropic, non-monotonic manner, which effectively replaces the cascade with particle–flow interactions. Particle clustering is also influenced by inertia in a non-monotonic manner, reaching a maximum when the Stokes number is of order unity. This produces concentration inhomogeneities that modulate energy transfer within the flow (Fornari *et al.*, 2016; Bec *et al.*, 2024; Hoque *et al.*, 2024; Chiarini & Rosti, 2024).

Reattachment downstream of a sudden expansion provides a controlled environment to assess the competing influences of particle-induced dissipation and diffusion, and their dependence on particle inertia, within a well-established flow topology. These assessments can then be related to other configurations, as the recirculation region encompasses a free shear layer, a bounded vortex region, and strong wall interactions. Previous studies have shown contrasting effects within this region. In Jeronimo & Rival (2021), increased particle loading dissipates instabilities in the shear layer, reducing entrainment of freestream fluid—a laminarizing effect. In contrast, Rosi *et al.* (2025) reported that increased loading yielded shorter reattachment lengths representative of turbulent sudden expansions, indicative of enhanced wallward momentum transfer through diffusion of shear-layer instabilities. These studies considered particles with density ratios of $\rho_\mathrm{p}/\rho_\mathrm{c} = 1/1$ and $7/1$, respectively, making direct comparison difficult. Accordingly, we investigate particle–wall interactions within the reattachment zone using particles spanning both density ratios. This approach clarifies how particle-induced dissipation and diffusion of shear-layer instabilities organizes along inertial lines, manifesting at the wall and affecting reattachment.

In this work, we observe phenomena that indicate how particle inertia organizes suspension dynamics into two regimes—a cascade-preserving dissipative regime and a cascade-redistributing diffusive regime—by investigating clustering, spreading, and near-wall transport in the reattachment region using velocity statistics, divergence, and Lagrangian diagnostics. The present investigation considers the motion of zinc and active-carbon microparticles, dilutely suspended in water and silicone oil, respectively, in the immediate downstream region of a vertical sudden expansion. Across Reynolds numbers and volume fractions, the results help reconcile the observations of Jeronimo & Rival (2021) and Rosi *et al.* (2025), with particle dynamics aligning with the two inertial regimes described in Chiarini & Rosti (2024). The following section describes suspension preparation, the sudden-expansion flow loop, imaging instrumentation, post-processing, and the test matrix. We then present velocity statistics, as well as spectral analyses of particle velocity divergence and forward finite-time Lyapunov exponent (f-FTLE) fields to reconcile the diffusive and dissipative mechanisms identified in the aforementioned studies within the reattachment zone.

METHODS

To investigate particle–wall interactions within the recirculation region, six dilute suspensions were prepared and tested in the flow loop shown in Fig. 1(a). The suspensions consisted of zinc in water and active-carbon in silicone oil, yielding wetted density ratios of $\rho_p/\rho_c = 7/1$ and $1/1$. The particles had mean diameters of 28 μm and 75 μm, corresponding to $O(0.01h)$, and exhibited a characteristic Stokes number of $Stk_h \sim O(10^{-3})$. Volume fractions of $\Phi = 1\%$, 3%, and 5% were prepared for both particle types. Experiments were conducted at carrier-phase Reynolds numbers of $Re_{d,carr} =$ 1000, 1500, and 2000 based on pipe diameter, with kinematic viscosities of 1.0×10^{-6} m^2/s for water and 2.0×10^{-5} m^2/s for silicone oil. All cases are matched by carrier-phase Reynolds number, allowing comparisons to be interpreted primarily through particle inertia.

Upon preparation, suspension mixtures were placed within the storage tank of the flow loop, which utilizes a 2:1 sudden expansion in a vertical acrylic pipe. The storage tank was continuously agitated to avoid settling. At the expansion, the flow is gradually constricted from the pipe diameter of $D = 21$mm to a throat diameter of $d = 10.5$mm by a pipe section whose inner diameter smoothly transitions from D to d using $d(s) = 0.5(d + (D-d)\sin(0.5\pi(s/d)))$. The setup included an 80D run-up and 20D recovery section to ensure fully developed flow. A high-speed camera (Phantom V40, 1 MP), viewing the pipe through a water-filled tank to minimize optical distortions, captured particle motion within a field of view spanning the full pipe width and sixteen step heights downstream of the expansion. For zinc, frame rates of 267, 400, and 600 Hz were matched to increasing Reynolds numbers, while frame rates of 6000, 9000, and 12000 Hz were used for active-carbon experiments, yielding particle displacements of roughly 5 px per frame at the wall.

Images were processed using the workflow illustrated in Fig. 1(b). The pipe domain was extracted, temporal mean intensity subtracted, and pixel columns shifted to linearize circumferential distance, with gaps filled using linear interpolation. Distorted image edges were masked, and the remaining image was processed using particle-image velocimetry (PIV) algorithms in DaVis 8.4.0 to obtain wall-bounded particle-velocity fields. The processing pipeline included mean-image subtraction, temporal and spatial Gaussian filtering (three frames, three pixels), and a multi-pass PIV algorithm with 75% window overlap (64×64 to 32×32 pixels). All reported quantities correspond to particle-phase velocities and represent near-wall kinematics, which may differ from carrier-phase dynamics. Streamwise velocity and fluctuation intensity are used to characterize mean transport and the amplitude of particle-fluid disturbances near the wall. Furthermore, the divergence field is used to quantify local clustering and spreading, while the forward FTLE identify Lagrangian ridges of repulsion that govern particle organization and transport.

RESULTS

Throughout the results, a clear distinction emerges between low- and high-inertia particles that organizes the dynamics along two regimes: a flow-coupled dissipative regime at low inertia and a flow-decoupled, diffusion-dominated regime at high inertia. Figs. 2 and 3 show the circumferentially averaged streamwise particle velocity and turbulent intensity as functions of downstream distance from the expansion for active carbon (a–c) and zinc (d–f), with plot titles indicating density ratio and throat-based Reynolds number. The streamwise particle velocity transitions from expansion-directed (negative) to downstream-directed (positive) within $6 \leq x/h \leq 14$, depending on the case. This transition coincides with the expected wall reattachment location (Pak *et al.*, 1990) and shifts upstream with increasing Reynolds number. It is accompanied by a reduction in near-wall particle velocities with increasing volume fraction (Aragall *et al.*, 2015). For low-inertia particles, the transition point is sensitive to Reynolds number and shifts downstream with increasing volume fraction, consistent with the shear-layer stabilization and laminarization observed in Jeronimo & Rival (2021). In contrast, for high-inertia particles, the transition point is comparatively insensitive to Reynolds number and volume fraction, though it shifts slightly upstream with increasing volume fraction, aligning with Rosi *et al.* (2025) and indicating enhanced wallward momentum transfer. For low-inertia cases, particle fluctuation intensity increases with Reynolds number but decreases monotonically with volume fraction, indicating attenuation of fluctuations without altering the overall flow structure and is consistent with preservation of the original scale-to-scale energy transfer. In contrast, high-inertia cases are largely insensitive to Reynolds number and exhibit a non-monotonic dependence on volume fraction, suggesting a shift away from flow-dominated dynamics toward particle–flow interactions. These results highlight the role of particle inertia in shifting the flow from a regime that preserves the original system dynamics to one dominated by particle–flow interactions.

The raw footage reveals clustering (convergence) and spreading (dispersion) events of particles along the pipe wall. To quantify these dynamics, the divergence of the pipe-wall-mapped particle velocity field was computed over time. Representative snapshots of the divergence field are shown in Fig. 4, with Re_d and Φ indicated in the column headers. The snapshots highlight clustering (negative) and spreading (positive) events convecting along the wall. For low-inertia cases, a transition is observed from small-scale, localized events to larger-scale coherent structures. In contrast, high-inertia cases exhibit clustering and spreading events of relatively consistent size, largely independent of volume fraction and Reynolds number. To quantify the scale and strength of these events, we examine spatial spectra of the divergence fields through the time-averaged, power-weighted circumferential wavelength, $\lambda_{(\nabla\cdot)}/h$ (Fig. 5), and RMS spectral power $(\nabla \cdot u)_{\mathrm{rms}}$ (Fig. 6), both as functions of streamwise distance. For low-inertia cases, the wavelength increases with Reynolds number and converges toward $\sim 1.6h$, while spectral power decreases with volume fraction and increases with Reynolds number. In contrast, high-inertia cases show nearly constant wavelength ($\sim 1.5h$) and weak, non-monotonic dependence on volume fraction, with little sensitivity to Reynolds number. Thus, low-inertia particles exhibit increasing wavelength and decreasing spectral power, indicating attenuation of small-scale structures while preserving the underlying large-scale flow structures. In contrast, high-inertia particles exhibit nearly constant wavelength and non-monotonic trends, reflecting decoupling from underlying flow structures and a transition toward a flow-structure behavior that is primarily particle-driven. We also examine these dynamics using finite-time Lyapunov exponent (FTLE) fields computed from the particle velocity fields. Typical forward FTLE snapshots are shown in Fig. 7. For low-inertia particles, ridges transition from tightly clustered to more broadly spaced, whereas for high-inertia particles, ridge spacing remains relatively uniform across Reynolds numbers and volume fractions. Temporal spectral analysis of the ridges shows that low-inertia particles exhibit lower Strouhal numbers and monotonic trends with volume fraction, while high-inertia particles exhibit non-monotonic behavior and increasing spectral power in the streamwise direction (Figs. 8, 9). These results reinforce that low-inertia particles preserve system dynamics while dissipating energy, whereas high-inertia particles disrupt system dynamics and drive it towards one dominated by the particles.

CONCLUSIONS AND OUTLOOK

This study suggests that particle inertia organizes near-wall suspension dynamics into two regimes: a system-preserving dissipative regime at low inertia and a system-disrupting regime at high inertia. This was done through an experimental investigation of particle-wall interactions within the reattachment zone downstream of a sudden expansion, spanning dilute volume fractions ($\Phi = 1\%,\ 3\%,\ 5\%$) and three Reynolds numbers ($\mathrm{Re}_d = 1000,\ 1500,\ 2000$), and reconciled the competing observations of particles promoting coherent-structure diffusion and dissipation, respectively reported by Rosi *et al.* (2025) and Jeronimo & Rival (2021) in sudden-expansion flows. In general, these competing effects fall along inertial lines, with low-inertia particles exhibiting monotonic trends in Reynolds number and volume fraction in mean velocity, divergence, and FTLE fields, pointing toward dissipative behavior that attenuates underlying flow structure yet preserves large-scale system behavior. Conversely, high-inertia particles exhibit weak sensitivity or non-monotonic behavior with Reynolds number and volume fraction, pointing to a transition from flow-driven behavior to particle-flow interactions that enhance energy transfer to smaller scales. This organization along inertia lines coincides with previous work on inertial effects on particle modulation of fluid flow (Fornari *et al.*, 2016; Bec *et al.*, 2024; Hoque *et al.*, 2024; Chiarini & Rosti, 2024), which collectively report how low-inertia particles maintain the original energy cascade within the flow, but is driven towards one dominated by particle-flow interactions by high inertia particles.

Despite the apparent organization along inertia-based trends suggested by our results, it is important to emphasize that the monotonic behavior observed in the low-inertia case, compared to the relative insensitivity and non-monotonicity of the high-inertia case, should not be interpreted as evidence that inertia alone can classify a suspension as exhibiting either momentum dissipation (a laminar-like characteristic) or rapid diffusion (a turbulent-like characteristic). Evidence of momentum diffusion has been reported in low-inertia suspensions (Barnes *et al.*, 2024; Fornari *et al.*, 2016), and prior work demonstrates that inertia alone is insufficient to distinguish whether a suspension attenuates or augments flow disturbances (Hoque *et al.*, 2024). Even in the present study, the growth in scale and intensity—alongside the streamwise weakening—of clustering and spreading events in the low-inertia case, as revealed by divergence and FTLE spectra, may reflect the concurrent diffusive growth of shear-layer structures. Conversely, the higher-frequency, shorter-wavelength events observed in the high-inertia case may instead result from the breakdown of shear-layer structures into smaller, weaker scales, i.e. dissipation. Placed in the context of previous work, these findings suggest that suspension systems do not simply drive the near-wall flow toward laminar or turbulent states, but are governed by inertia-dependent mechanisms that redistribute energy, either dissipating while preserving dominant scales or disrupting and diffusing them.

REFERENCES

Aragall, R., Mulchandani, V. & Brenner, G. 2015 Optical measurement and numerical analysis of mono- and bidisperse coarse suspensions in vertical axisymmetric sudden-expansion. *International Journal of Multiphase Flow* **69**, 63–80.

Barnes, M., Zhang, K. & Rival, D. 2024 Lagrangian study of entrainment for confined vortex rings in dense suspensions using echo-lpt. *Experiments in Fluids* **65** (3).

Bec, J., Gustavsson, K. & Mehlig, B. 2024 Statistical models for the dynamics of heavy particles in turbulence. *Annual Review of Fluid Mechanics* **56** (1), 189–213.

Chiarini, A. & Rosti, M. E. 2024 Finite-size inertial spherical particles in turbulence. *Journal of Fluid Mechanics* **988**, A17.

Druzhinin, O. A. 1994 Concentration waves and flow modification in a particle-laden circular vortex. *Physics of Fluids* **6** (10), 3276–3284.

Fornari, W., Formenti, A., Picano, F. & Brandt, L. 2016 The effect of particle density in turbulent channel flow laden with finite size particles in semi-dilute conditions. *Physics of Fluids* **28** (3).

Guazzelli, É. & Pouliquen, O. 2018 Rheology of dense granular suspensions. *Journal of Fluid Mechanics* **852**.

Hogendoorn, W. & Poelma, C. 2018 Particle-laden pipe flows at high volume fractions show transition without puffs. *Physical review letters* **121** (19), 194501.

Hoque, M. M., Joshi, J. B., Evans, G. M. & Mitra, S. 2024 A critical analysis of turbulence modulation in particulate flow systems: a review of the experimental studies. *Reviews in Chemical Engineering* **40** (4), 511–544.

Jeronimo, M. D. & Rival, D. E. 2021 On the lifespan of recirculating suspensions with pulsatile flow. *Journal of Fluid Mechanics* **928**.

Kiger, K. T. & Pan, C. 2002 Suspension and turbulence modification effects of solid particulates on a horizontal turbulent channel flow. *Journal of Turbulence* **3**, N19.

Pak, B., Cho, Y. I. & Choi, S. U. S. 1990 Separation and reattachment of non-newtonian fluid flows in a sudden expansion pipe. *Journal of Non-Newtonian Fluid Mechanics* **37** (2-3), 175–199.

Richter, D. H. & Sullivan, P. P. 2014 Modification of near-wall coherent structures by inertial particles. *Physics of Fluids* **26** (10).

Rosi, G., Barnes, M., Kaiser, F. & Rival, D. E. 2025 Exploring separation and reattachment in shear-thinning suspensions through pipe-wall ultrasound measurements. *Experiments in Fluids* **66** (5), 99.

Shuai, S. & Kasbaoui, M. H. 2022 Accelerated decay of a lamb–oseen vortex tube laden with inertial particles in eulerian–lagrangian simulations. *Journal of Fluid Mechanics* **936**.

Stickel, J. J. & Powell, R. L. 2005 Fluid mechanics and rheology of dense suspensions. *Annual Review of Fluid Mechanics* **37**, 129–149.

Zhang, K. & Rival, D. E. 2020 On the dynamics of unconfined and confined vortex rings in dense suspensions. *Journal of Fluid Mechanics* **902**.

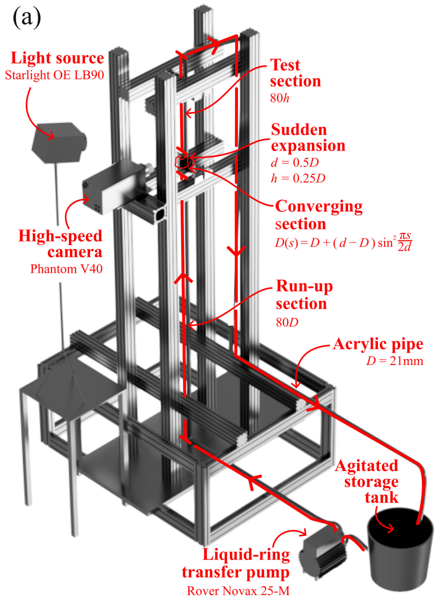

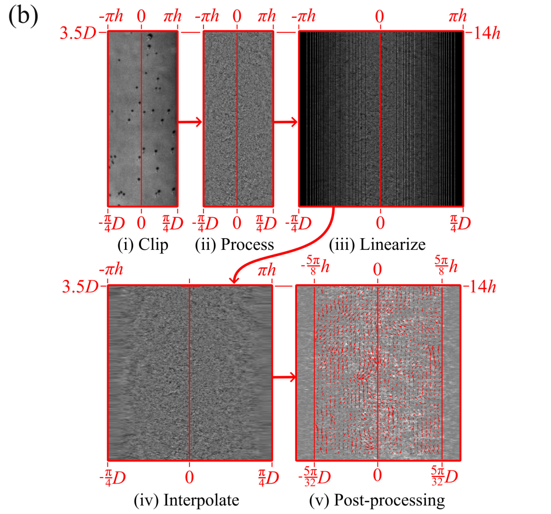

(c)

Particle / Carrier	d_p/h ($\times 10^4$)	ρ_c/ρ_p	Φ (%)	Re_d
Zinc / Water	9.5	1/7	1, 3, 5	1000, 1500, 2000
Carbon / Silicone Oil	14.3	1/1		

Figure 1: (a) Sudden vertical expansion with annotations indicating key equipment and geometries. (b) Workflow to generate vectors from particle images. (c) Summary of test matrix.

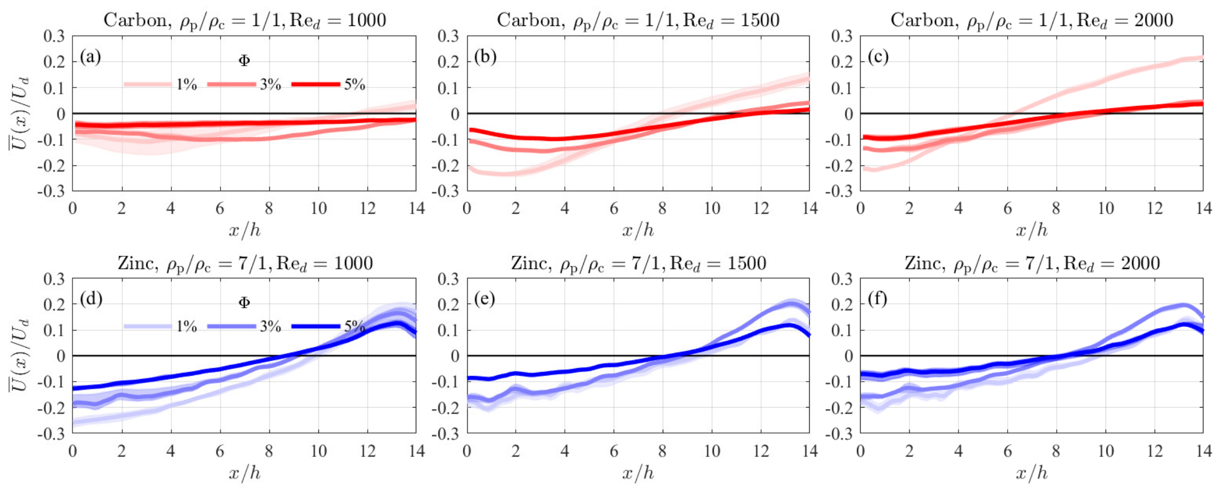

Figure 2: Mean streamwise velocity of wall-bounded particles vs. distance from the expansion.

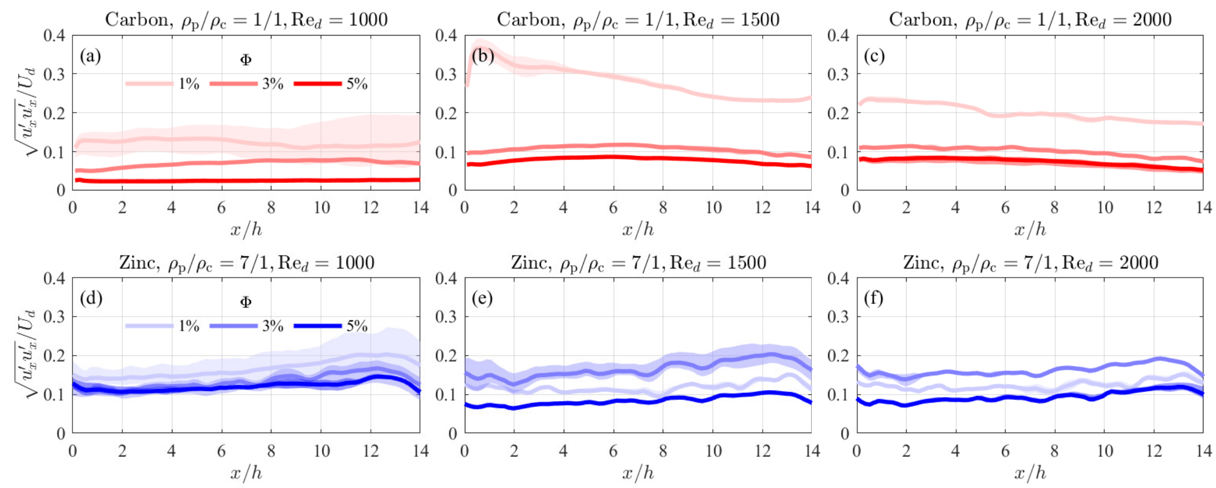

Figure 3: Streamwise fluctuation intensities of wall-bounded particles vs. distance from the expansion.

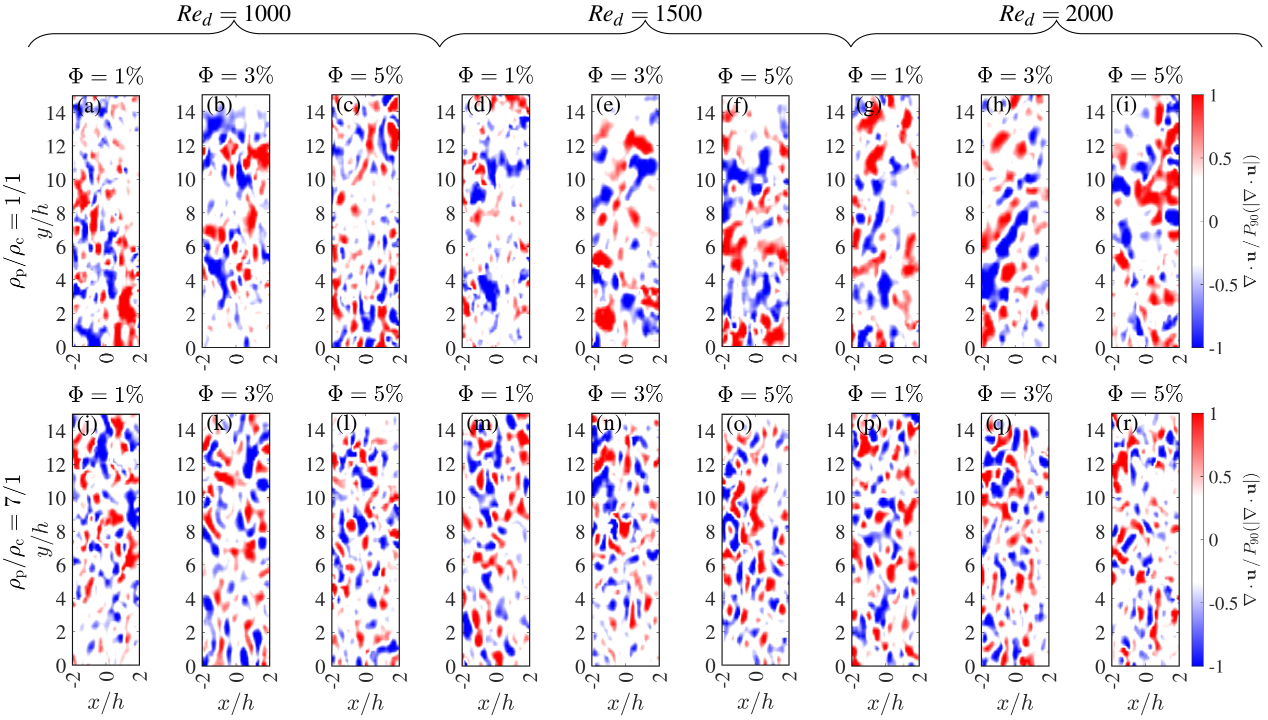

Figure 4: Representative instances of particle divergence, normalized by the ninetieth percentile event over the entire run.

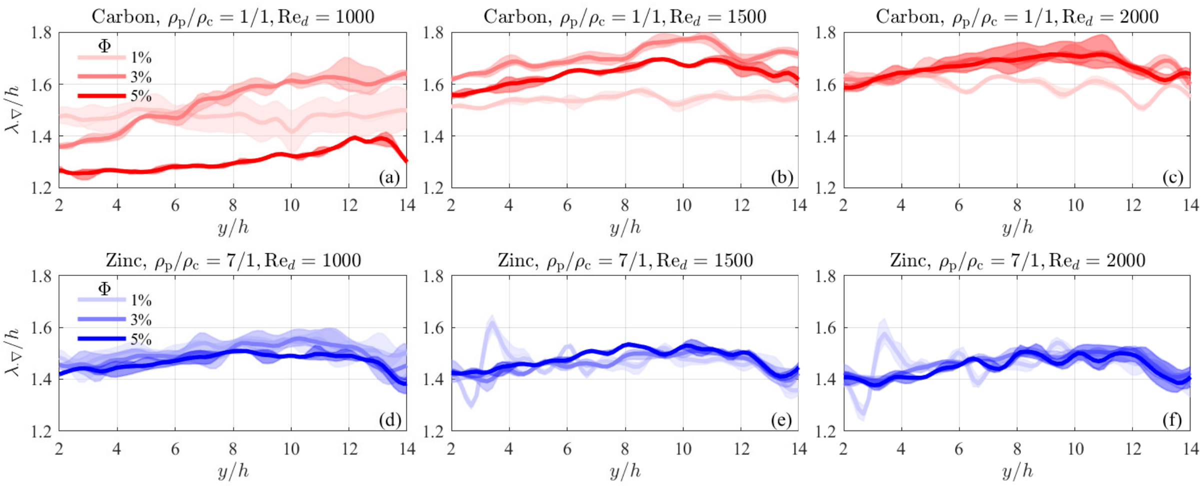

Figure 5: Circumferentially averaged, power-weighted wavelength of the spatial spectra of divergence along pipe.

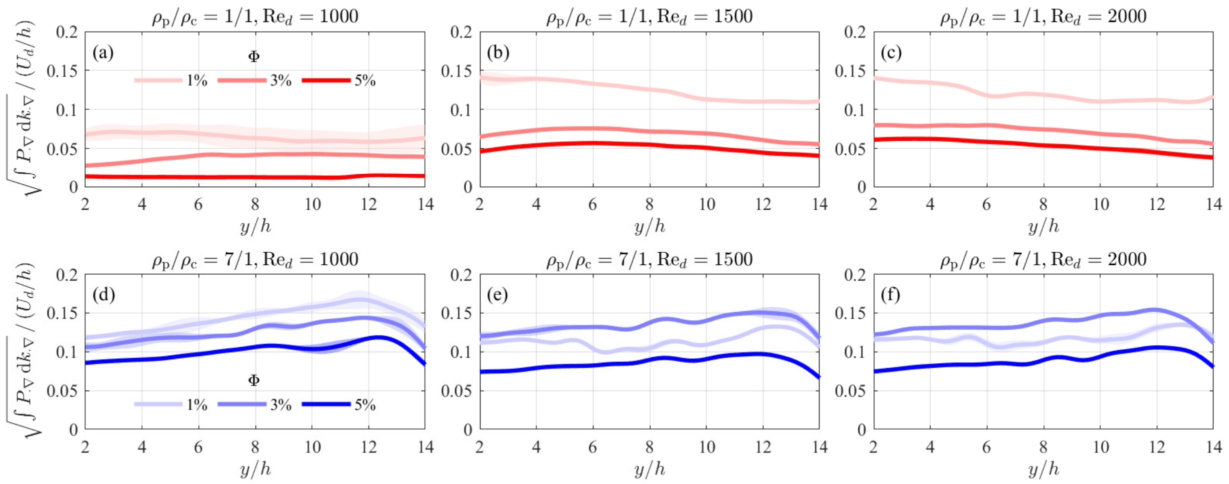

Figure 6: Circumferentially averaged, root-mean square of spectral power of particle divergence along pipe.

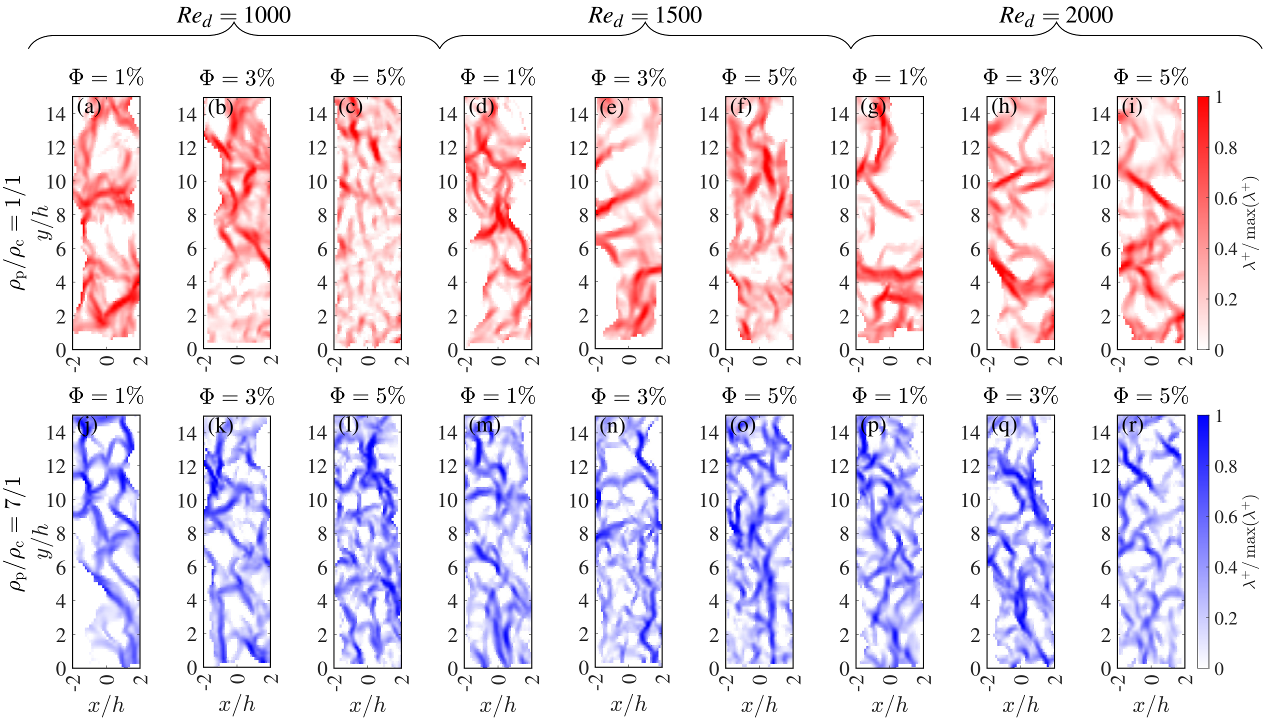

Figure 7: Representative instances of forward FTLE fields, integrating over half a shedding cycle with $St = 0.1$.

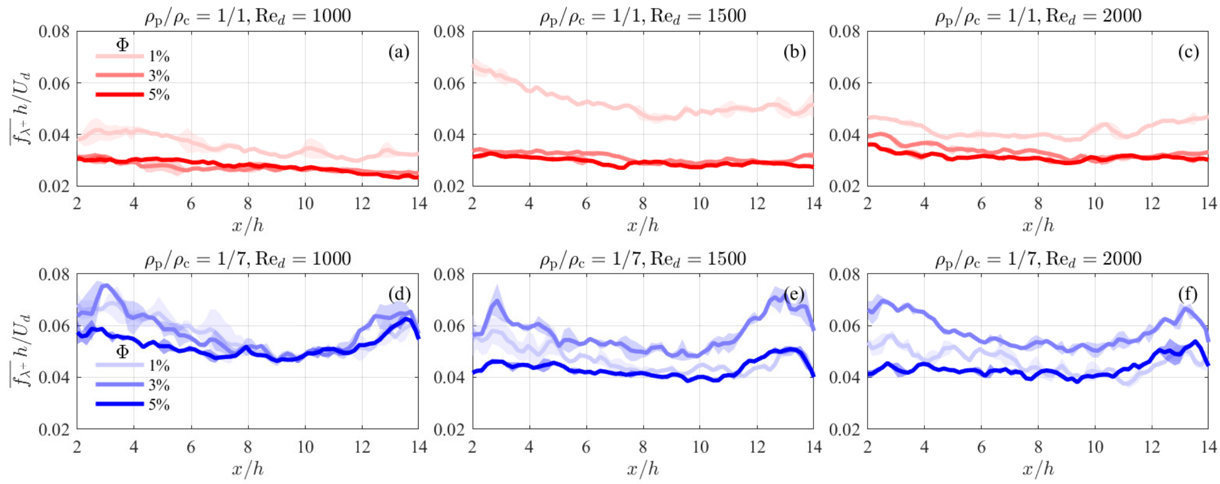

Figure 8: Circumferentially averaged, power-weighted Strouhal number of the fFTLE temporal spectra along pipe.

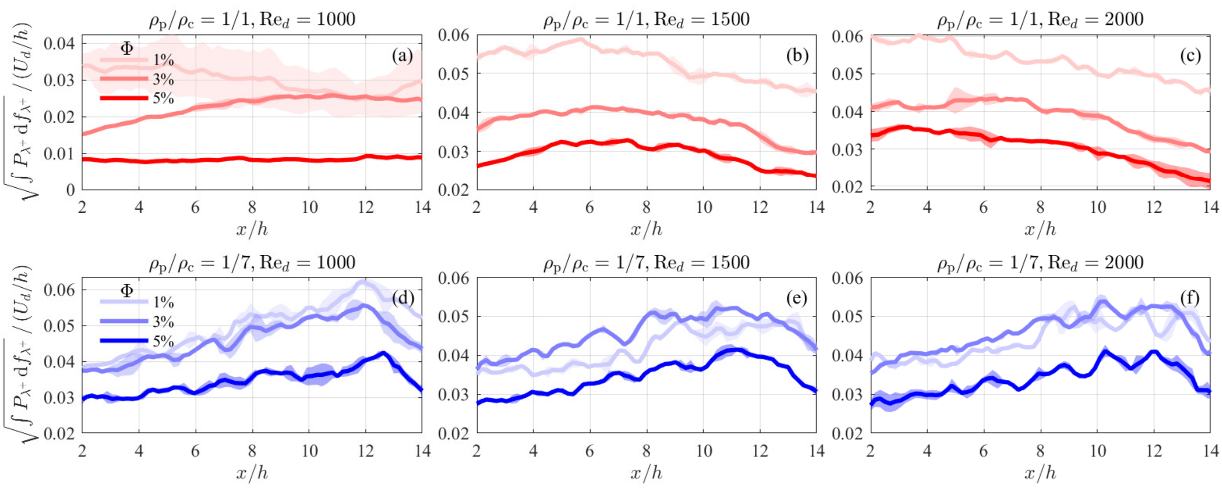

Figure 9. Circumferentially averaged, root-mean-square of the temporal spectral power in the fFTLE fields along the pipe.